Mechanism of internal modification in bulk borosilicate glass with picosecond laser pulses at high repetition rates

Conference Paper *in* Proceedings of SPIE - The International Society for Optical Engineering · May 2015

DOI: 10.1117/12.2185518

CITATION
1

READS
107

4 authors, including:

Mingying Sun
Shanghai Institute of Optics and Fine Mechanic…
16 PUBLICATIONS **26** CITATIONS
SEE PROFILE

Wolfgang Schulz
Fraunhofer Institute for Laser Technology ILT
112 PUBLICATIONS **747** CITATIONS
SEE PROFILE

Mechanism of internal modification in bulk borosilicate glass with picosecond laser pulses at high repetition rates

Mingying Sun[a,*], Urs Eppelt[b, c], Wolfgang Schulz[b, c], and Jianqiang Zhu[a]
[a]Shanghai Institute of Optics and Fine Mechanics, Chinese Academy of Sciences, Qinghe Road 390, Jiading District, Shanghai 201800, China;
[b]Fraunhofer-Institut für Lasertechnik, Steinbachstr. 15, 52074 Aachen, Germany;
[c]Nonlinear Dynamics of Laser Processing, RWTH Aachen University, Steinbachstr. 15, 52074 Aachen, Germany

ABSTRACT

We present a numerical model of internal modification in bulk borosilicate glass by high repetition rate picosecond laser pulses. We study free-electron dynamics, nonlinear energy deposition and thermal conduction. The optical absorptivity and modification regions both have good agreements with the experimental results. The smooth outer zone is the molten region and the inner-structure formation is caused by high-density free-electrons generated by thermal ionization. Excitation, relaxation and accumulation of free-electron density in the focal volume are analyzed using different pulse shapes and a double-pulse train. The deposited energy distribution and modification zone are controlled by pulse shaping.

Keywords: Laser damage; Laser-induced breakdown; Glass and other amorphous materials; Ultrafast lasers; Laser materials processing; Picosecond phenomena.

1. INTRODUCTION

The internal modification of transparent dielectrics by high repetition rate ultra-short lasers becomes highly attractive in various applications of micromachining[1] such as waveguide writing[2-7] and microwelding[8-13]. When ultra-short laser pulses are tightly focused inside transparent dielectrics, laser pulse energy is nonlinearly absorbed through generating and heating free-electrons and then transferred to the lattice to heat the material. When the time interval between successive pulses is less than thermal diffusion time, the temperature in the focal volume rises up to several thousand degrees[14-16] because of heat accumulation. The re-solidification of the molten material leads to refractive index change or micro-joining. The nonlinear absorption of laser pulses provides the localized modification in micro/nanometer scale. Although the internal modifications in bulk transparent dielectrics have been beautifully demonstrated in experiments[2-13], the modification mechanisms are not clearly understood yet, which needs more theoretical and numerical studies.

Several numerical models for heat accumulation and internal modification of transparent dielectrics by ultra-short laser pulses at high repetition rates have been reported. Thermal conduction models[3, 13, 14, 17, 18] were widely used to calculate time-dependent temperature distributions and determine the size of the heat affected zone. In the models, the heat source was usually assumed as a Gaussian distribution[3, 14, 17, 18] or a cylindrical distribution[13]. Miyamoto et al.[9, 10] presented thermal conduction models for steady and transient temperature distributions and evaluated the nonlinear absorptivity in the internal modification of borosilicate glass by picosecond laser pulses, whereas the heat source was determined by fitting the resulting isotherms to the experimental results. In principle, the heat source distribution can be calculated from the laser-induced plasma formation and energy deposition. Nonlinear plasma generation[19-22] and energy deposition[23, 24] in bulk transparent dielectrics irradiated by single ultra-short laser pulse have been numerically investigated. For internal modifications by high-repetition-rate ultra-short laser pulses, however, theoretical and numerical studies based on beam propagation and nonlinear ionization are still rare.

This study presents a numerical model to study the internal modification in bulk glass irradiated by high repetition rate picosecond laser pulses. The model contains a rate equation for the free-electron density, a laser transport equation and a thermal conduction equation. Simulations are performed to study the plasma formation, nonlinear energy deposition, temperature distribution and modifications in bulk glass. We analyze the influences of pulse shape and double-pulse trains on free-electronic excitation, relaxation and accumulation and thereby on the internal modification of bulk glass. At last the mechanisms of electronic and heat accumulation are discussed based on thermal ionization.

Pacific Rim Laser Damage 2015: Optical Materials for High-Power Lasers, edited by Jianda Shao, Takahisa Jitsuno, Wolfgang Rudolph, Proc. of SPIE Vol. 9532, 953214 · © 2015 SPIE
CCC code: 0277-786X/15/$18 · doi: 10.1117/12.2185518

2. NUMERICAL MODEL

In the numerical model of internal modification, nonlinear energy deposition of laser pulses is determined by a plasma model and a transport equation for laser beam. Using the deposited energy as a heat source, we apply a thermal conduction model to calculate the temperature distribution, based on which heat modification regions are estimated.

2.1 Nonlinear energy deposition

In transparent dielectrics, strong electric fields excite the electrons in the valence band to be free electrons via photo-ionization and cascade ionization. The temporal evolution of free-electron density ρ is described by a rate equation[18, 22, 25] like

$$\frac{\partial \rho(z,t)}{\partial t} = \eta_{\text{photo}} + \eta_{\text{casc}}\rho(z,t) - \eta_{\text{rec}}\rho(z,t)^2, \tag{1}$$

where the terms on the right side denote the rates for photo-ionization, cascade ionization and recombination, respectively, and η_{photo}, η_{casc} and η_{rec} are the corresponding coefficients. The laser intensity used in this study is smaller than 2×10^{12} W/cm^2 and the Keldysh parameter[18, 25] is larger than 2.5. Thus multi-photon ionization (MPI) rather than tunneling ionization dominates in the photo-ionization process[25]. The MPI rate is taken from the Kennedy's approximation[26] of the Keldysh model, i.e.

$$\eta_{\text{photo}} = \frac{2\omega}{9\pi}\left(\frac{m\omega}{\hbar}\right)^{3/2}\left(\frac{e^2}{16\omega^2 c\varepsilon_0 n_0 m E_{\text{g}}} I(z,t)\right)^k \exp[2k]\cdot\Phi\left[\left(2k - 2\frac{E_{\text{g}}}{\hbar\omega}\right)^{1/2}\right], \tag{2}$$

where ω is the laser angular frequency, m is the reduced mass of electron-hole pair, $\hbar$ is the reduced Planck constant, e is the electron charge, c is the light speed in vacuum, ε_0 is the vacuum dielectric permittivity, n_0 is the refractive index of the dielectrics, and E_{g} is the band-gap of the dielectrics. $I(z, t)$ is laser intensity, Φ is the Dawson probability integral[18] and k is the photon number for MPI and equals to the integer part of $(E_{\text{g}}/\hbar\omega+1)$. The cascade ionization coefficient[26] is given by

$$\eta_{\text{casc}} = \frac{1}{\omega^2\tau^2+1}\left[\frac{e^2\tau}{cn_0\varepsilon_0 m_{\text{e}} E_{\text{crit}}} I(z,t) - \frac{m_{\text{e}}\omega^2\tau}{M}\frac{2E_{\text{av}}}{E_{\text{crit}}}\right], \tag{3}$$

where τ is the electron collision time, m_{e} is the electron mass, $m_{\text{e}} = 2\,m$, and M is the mass of atom/molecular. $E_{\text{crit}} = 1.5\,E_{\text{g}}$ [18] is the critical kinetic energy of the heated electrons for impact ionization. $E_{\text{av}} = 2.25\,E_{\text{g}}$ [18] is the average energy of free-electrons, which is the sum of the kinetic energy and the band-gap.

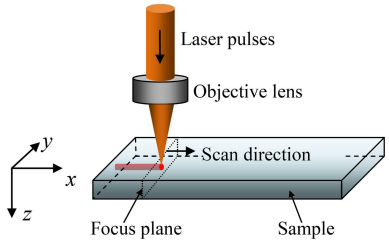

Figure 1. Schematic for the internal modification of glass sample with picosecond laser pulses at high repetition rates.

The schematic diagram of the setup is shown in Fig. 1. The scan speed v of laser beam is much smaller than the light speed c/n_0; therefore laser pulse propagation in glass can be described by a transport equation

$$\frac{1}{c/n_0}\frac{\partial I(z,t)}{\partial t} + \frac{\partial I(z,t)}{\partial z} = -\alpha(z,t)I(z,t) - \frac{2(z-z_{\text{f}})}{z_{\text{R}}^2 + (z-z_{\text{f}})^2} I(z,t), \tag{4}$$

where z_{R} and z_{f} are the Rayleigh length and focus position of the laser beam, respectively, and $\alpha(z,t)$ is the total absorption coefficient given by

$$\alpha(z,t) = \left(\eta_{\text{photo}} + \eta_{\text{casc}}\rho(z,t)\right)\cdot E_{\text{av}} \Big/ I(z,t). \tag{5}$$

The absorption coefficient induced by MPI is $\alpha_{\text{MPI}}(z,t) = \eta_{\text{photo}}E_{\text{av}}/I(z,t)$, which is only dependent on the laser intensity, and the remaining part of $\alpha(z,t)$ is caused by cascade ionization and thus determined by the free-electron density. Therefore nonlinear absorption dynamics of laser energy and absorptivity of the dielectrics can be evaluated numerically. The top surface of the sample is located at $z = 0$ and the sample thickness is d. The laser pulse shape is a Gaussian profile $I(0, t) = I_0 \exp[-4 \ln 2 (t - n_0 z_f/c - 2t_p)^2/ t_p^2]$, where t_p is the pulse duration and I_0 is the peak intensity. As the interaction volume is far away from the sample surfaces, the Fresnel reflections on the surfaces are negligible as well as the scattering of laser light[9] in the interaction volume.

2.2 Heat source and thermal conduction

When an ultra-short pulse is tightly focused inside the bulk glass, the laser energy is absorbed via MPI and inverse bremsstrahlung process as described by Eqs. (1) and (4). The deposited energy is firstly carried by free-electrons and then heats the lattice through electron-phonon collision, resulting in thermal diffusion and heat modification.

One-dimensional numerical simulation of plasma dynamics and nonlinear energy deposition along the z axis is performed at the center of laser beam spot, i.e. $y = 0$ μm. It is assuming that all the energy of the free-electrons is transferred to the lattice and induces thermal effects. That is, the energy gained by the free-electrons from the laser pulse serves as the heat source for thermal diffusion. Thus by integrating the nonlinear absorption coefficient in Eq. (5), the volume density distribution of the deposited energy of an individual laser pulse along the z axis is calculated as

$$Q_{\text{v}}(z) = \int_0^{\infty} \alpha(z,t) I(z,t)\, \mathrm{d}t. \tag{6}$$

The deposited energy distribution on the x-y plane induced by ultra-short laser pulses is approximately proportional to $I(z,t)$ [3, 9, 13, 17] because of avalanche ionization and heat accumulation. Since the beam size in the focus region is much smaller than the heat affected zone, the line density of the deposited energy is treated as a line heat source, which is calculated by integrating $Q_{\text{v}}(z)$ on the transverse plane as

$$Q_{\text{l}}(z) = \pi w(z)^2 \cdot Q_{\text{v}}(z), \tag{7}$$

where $w(z) = w_0[1+(z-z_f)^2/z_R^2]^{1/2}$ is the beam size distribution along the z axis, and w_0 is the beam waist.

When a pulsed laser at a repetition rate f_{rep} scans from $x = -\infty$ at a constant speed v along the x axis in bulk glass, where $w_0/v >> 1/f_{\text{rep}}$, the deposited energy can be treated as a continuous heat delivery. The material characteristics, e.g. temperature distributions, at the writing/welding front keep in a constant state for successive pulses[16] and the resulting modification channel along the x axis is homogenously distributed with a constant diameter[1, 3, 6, 27]. That means, the interactions of the focal volume with successive pulses are approximately the same and produce the identical deposited energy distribution $Q_{\text{l}}(z)$ by each pulse. Thus the continuous heat delivery is given by the line power density $f_{\text{rep}}\, Q_{\text{l}}(z)$ and the steady temperature distribution in the three-dimensional space is calculated by [9]

$$T(x,y,z) = \frac{1}{4\pi\lambda_{\text{c}}} \int_0^d \frac{f_{\text{rep}} Q_{\text{l}}(z')}{r} e^{-\frac{v}{2\kappa}(x+r)}\, dz' + T_0, \tag{8}$$

where T_0 is the initial temperature of the dielectrics, $r = [x^2+y^2+(z-z')^2]^{1/2}$, $\kappa = \lambda_{\text{c}}/(n_{\text{M}} \cdot c_{\text{p}})$ is thermal diffusivity, λ_{c}, n_{M} and c_{p} are thermal conductivity, mass density and specific heat capacity of the dielectrics, respectively.

Using the line density distribution $Q_{\text{l}}(z)$ of the deposited energy of an individual pulse, one can evaluate the absorbed energy and the absorptivity. When the incident pulse energy is E_{p}, the absorptivity A is defined as the ratio of the absorbed energy to the pulse energy, i.e.

$$A = \int_0^d Q_{\text{l}}(z)\, \mathrm{d}z \Big/ E_{\text{p}}. \tag{9}$$

2.3 Laser and material parameters

In the numerical simulation, a 1064nm, 10ps, 500 kHz pulsed laser is focused at z_f = 150 μm in the sample by an objective lens (NA = 0.55), as shown in Fig. 1. The sample is a borosilicate glass (Schott D263) with a thickness d of 200 μm. The beam quality factor M^2 = 1.1. The scan speed v is 20 mm/s. The beam waist in the material is 3.3μm. The pulse energy E_p varies from 0.1 μJ to 2.46 μJ. Material parameters of the sample[9, 28]: the refractive index n_0 is 1.52, the band-gap E_g is 3.7 eV, the thermal conductivity λ_c is 0.96 W/(m·K), the mass density n_M is 2.51×10^3 kg/m^3, the specific heat capacity c_p is 0.82×10^3 J/(kg·K) and the initial temperature T_0 is 25 °C.

The relaxation of laser-induced electron plasma in dielectric materials depends on the free-electron density. The lifetime of laser-induced plasma in Soda Lime and K9 glasses[29] increases from several ps to 100 ps when the plasma density is decreasing. The used borosilicate glass has the similar quality with K9 glass[25], thus a two-body recombination mechanism is used in the plasma model in Eq. (1). The recombination rate η_{rec} is taken as 2×10^{-9} cm^3/s to obtain the plasma lifetime $1/(\eta_{rec}\rho)$ from 5 ps to 100 ps when the free-electron density ρ is decaying from 10^{20} cm^{-3} to 5×10^{18} cm^{-3}. The electron collision time τ in transparent dielectrics is several fs [18-25, 29, 30] and τ = 4 fs in the simulations.

2.4 Modification criteria

For laser wavelength of 1064nm, the critical free-electron density for laser breakdown[18] is $\rho_{crit} = \omega^2 m_e \varepsilon_0 / e^2 = 1.0\times10^{21}$ cm^{-3}. The free-electron density corresponding to the damage threshold in glasses[19, 24, 25] is $\rho_d = 10^{20}$ cm^{-3}, above which the material is modified because of the energy released from high-density free-electrons, so called electronic damage or modification[25] in this paper. The term "electronic damage/modification" denotes an ablation mechanism based on the free-electron density rather than on the temperature. We distinguish it from thermal damage/ablation, but do not specify exactly what this damage means on the chemistry level. ρ_d is used as the criterion for the electronic modification here.

The deposited energy mediated by the free-electrons results in a temperature rise in the interaction volume. Due to the slow scan and high repetition rate of the laser source, the spatial overlap $1\text{-}v/(2w_0 f_{rep})$ of adjacent pulses is 99.4% and there are more than one hundred laser pulses hitting the same spot with a size of $2w_0$. The temperature T increases with pulse number because of heat accumulation and the material is modified because of visco-elastic deformation and glass element flow[17, 31]. Firstly, we follow the assumptions of the modification criteria proposed by Miyamoto el al. [9] that the isothermal lines at T_m = 1051 °C and T_b = 3600 °C are the boundaries of two different heat modification regions. T_m is referred as the melting temperature and T_b is a fitting temperature to reproduce the contour of the inner structure in the internal modification. Therefore the heat modification criteria in this paper are that the area where the temperature $T > T_b$ is the inner structure while the zone where $T_m < T < T_b$ is the outer molten region. Secondly, the choice of T_b is explained based on the numerical and experimental results and meanwhile, the roles of electronic and heat modification in the internal modification of bulk glass are compared.

3. MECHANISM OF INTERNAL MODIFICATION

3.1 Plasma dynamics and energy deposition

Using the numerical model, we analyze the internal interaction process in bulk glass irradiated by picosecond laser pulses with pulse energy E_p = 2.46 μJ, including nonlinear absorption of photons, plasma formation and energy deposition. Figure 2(a) shows laser-induced free-electron density distributions along the z axis at different time instants. The laser pulse is a Gaussian profile and converges before arriving at the focus, so the leading-edge of the laser pulse produces high-density free-electrons at the focus firstly. For the subsequent portion of the laser pulse, the plasma formation front moves towards the laser source. Therefore the laser intensity after t = 15 ps is consumed before arriving at the focus as shown in Fig. 2(b). Figure 2(c) shows that the total absorption coefficient α along the z axis at different time instants is proportional to the corresponding free-electron density. The absorption coefficient α_{MPI} induced by MPI given in Fig. 2(d) is smaller than α by four orders of magnitude; thus cascade ionization is dominant in the nonlinear absorption of laser energy.

In order to study the electronic damage, the maximum free-electron density ρ_M during the ionization process along the z axis is obtained as shown in Fig. 2(e). The electronic modification forms in the area where $\rho_M > \rho_d$. So the length of the electronic damage region is calculated to be 68 μm, which will be compared in Section 3.3 to the inner structure length of the modification region observed in the experiment and predicted by the temperature T_b.

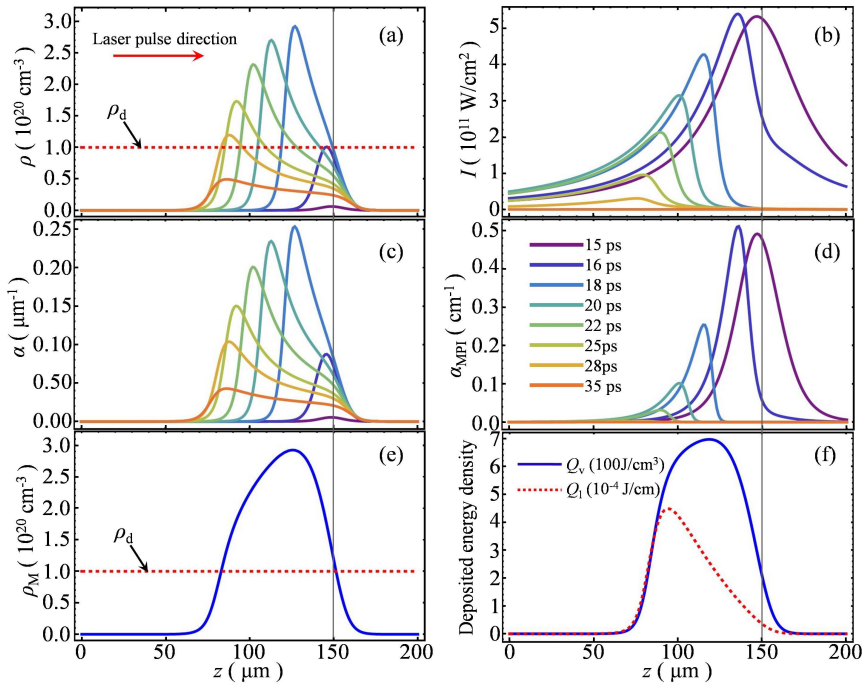

Figure 2. Distributions of (a) free-electron density ρ, (b) laser intensity I, (c) total absorption coefficient α and (d) absorption coefficient α_{MPI} induced by MPI, along the z axis at different time instants. Distributions of (e) maximum free-electron density ρ_M during the ionization process and (f) volume density Q_v and line density Q_l of the deposited energy along the z axis. Laser pulse energy of 2.46 μJ is used. (a) – (d) have the same legend as that shown in (d). The red arrow indicates the laser incident direction. The focus of laser beam is located at z =150 μm indicated by a thin gray line.

The volume density Q_v and the line density Q_l of the deposited energy along the z axis calculated with Eqs. (6) and (7) are shown in Fig. 2(f). Due to the plasma expansion towards the laser source, the peak of the volume density along the z axis is in front of the focus. The line density distribution is an approximately triangular profile because of the tight focus and its peak is located at z = 100 μm. By integrating $Q_l(z)$ from z = 0 to d, the absorbed energy is calculated to be 1.92 μJ. Thus with Eq. (9), the absorptivity A is evaluated to be 78%.

3.2 Temperature distribution

The simulated line density Q_l of the deposited energy along the z axis in bulk glass irradiated by laser pulses with various pulse energies are shown in Fig. 3(a). At the threshold case (E_p = 0.41 μJ), the energy distribution is located near the focus. When E_p > 0.41 μJ, due to the larger peak intensity, the deposited energy distribution expands towards the laser source with the similar profile and the absorbed energy increases. Using Eq. (9) and the data in Fig. 3(a), the absorptivity A of the dielectrics is calculated as a function of pulse energy E_p as shown in Fig. 3(b). The absorptivity A increases with E_p and finally gets almost constant, which agrees well with results given by the experiment and model in Ref. [9].

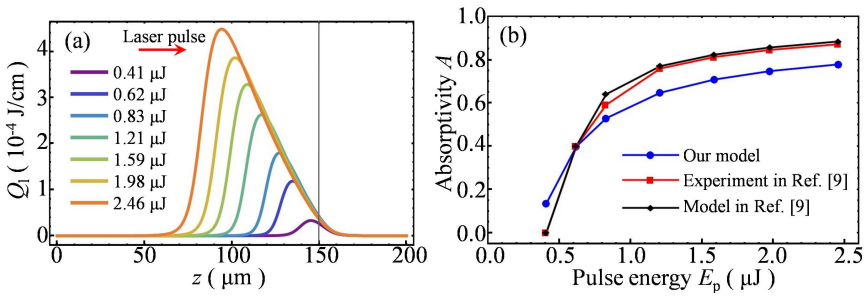

Figure 3. (a) Simulated line density Q_l of the deposited energy along the z axis in bulk glass irradiated by laser pulses with different pulse energies. (b) Absorptivity A as a function of pulse energy E_p given by our numerical model, the experiment and model in Ref. [9]. In (a), the red arrow indicates the laser incident direction and the focus of laser beam is located at z=150 μm indicated by a thin gray line.

Using the deposited heat source Q_l in Fig. 3(a) and the heat conduction model in Eq. (8), we obtain the cross-sections of temperature distribution in the steady state at different pulse energies as shown in Fig. 4(a). The maximum temperature on the cross section increases with pulse energy E_p and it is larger than 6000 °C when E_p >1.21 μJ. This is consistent with the Raman temperature measurements[15] and the temperature estimation based on the transient refractive index change measurement[16]. The high temperature region (e.g. T > 1000 °C) extends along the y direction because of more absorbed energy and along the z direction because of the heat source expansion towards the laser.

Based on the temperature distribution in Fig. 4(a), two different heat modification regions are defined by the two isothermal lines (T_m and T_b), as shown in Fig. 4(b). The outer and inner contours are both smooth and regular because of heat diffusion. The simulated cross-sections of the internal modifications in bulk glass have great agreements with the experimental results[9] in Fig. 4(c) in a wide range of pulse energy. It is widely considering that the outer modified region is the molten area[9-12]. The different morphology of the inner structure, however, indicates another modification mechanism.

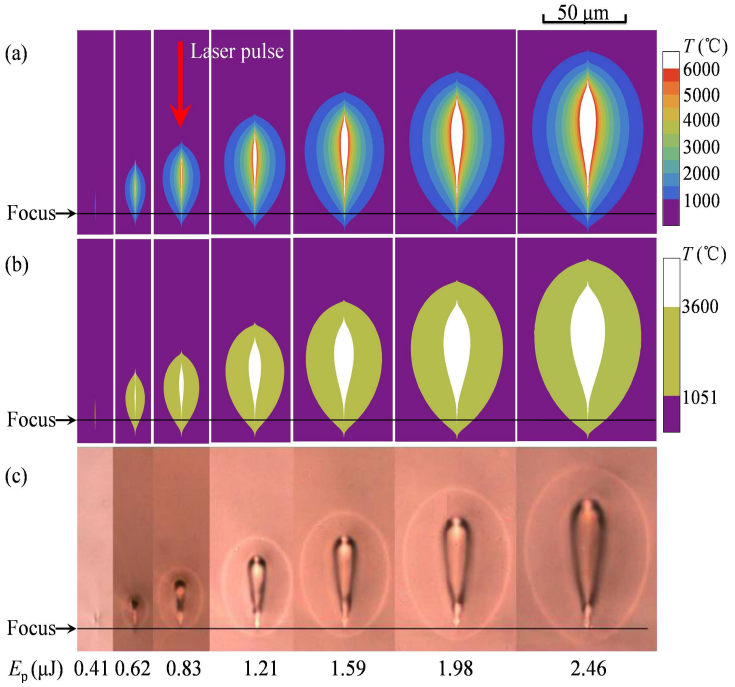

Figure 4. Cross-sections of (a) simulated temperature distribution and (b) simulated modification regions defined by two isothermal lines (T_m = 1051 °C and T_b = 3600 °C) and (c) internal modification in the reported experiment in Ref. [9] at different pulse energies. The red arrow indicates the laser incident direction. The focus of laser beam is indicated by horizontal lines.

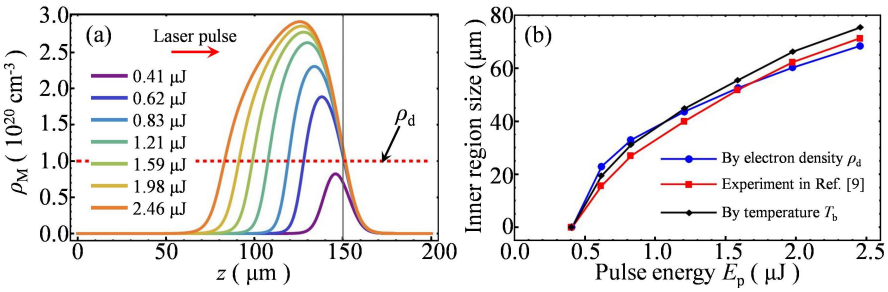

Figure 5. (a) Distributions of maximum free-electron density ρ_M along the z axis in bulk glass irradiated by laser pulses with different pulse energies. (b) Size comparison of the inner structure in the modification region along the z axis defined by the free-electron density ρ_d and by the temperature T_b as well as the experimental measurement[9] at various pulse energies E_p. In (a), the red arrow indicates the laser incident direction and the focus of laser beam is located at z =150 μm indicated by a thin gray line.

3.3 Electronic damage and thermal damage

The distributions of the maximum free-electron density ρ_M during the ionization process along the z axis in bulk glass irradiated by laser pulses with various pulse energies are obtained as shown in Fig. 5(a). At the threshold case (E_p = 0.41 μJ), $\rho_M < \rho_d$, thus no electronic modification occurs. When $E_p > 0.41$ μJ, the peak of the maximum free-electron density exceeds ρ_d and the laser-induced plasma expands towards the laser source because of the larger peak intensity. Therefore the length of the electronic damage region, where $\rho_M > \rho_d$, is increasing with pulse energy, whereas the lower end is always located at the focus as observed in the experiment (see Fig. 4).

Figure 5(a) shows that the maximum free-electron density in the internal modification of bulk glass saturates around 3×10^{20} cm^{-3} when the pulse energy E_p increasing from 0.41 μJ to 2.46 μJ. The saturating peak density is well below the critical free-electron density ρ_{crit} for laser breakdown[19]. Therefore the transient refractive index change because of the presence of free-electron density[32] is minimal and thereby the in process reflection and diffraction induced by the plasma can be neglected in the internal modification.

In order to determine the damage mechanism of the inner structure in the internal modification region, in Fig. 5(b) we compare the sizes (along the z axis) of the electronic damage track defined by the damage threshold density ρ_d and the inner modification region defined by the temperature T_b as well as the inner structure measured in the experiments[9]. The length estimations of the inner structure based on the electronic and heat modifications both have good agreements with the experimental results. Therefore the electronic damage and heat modification induced by temperatures larger than T_b seem to be consistent. In order to understand its physical picture, we study the free-electron excitation, relaxation and accumulation in the following section and give an explanation based on thermal ionization.

4. FREE-ELECTRON EXCITATION, RELAXATION AND ACCUMULATION

In Section 3, the numerical model is verified by the agreement between the numerical and experimental results. Based on this model, we study the effect of pulse shape and a double-pulse train on the internal modification of bulk glass with high repetition rate picosecond laser pulses. The relaxation and accumulation of free-electron density are studied by varying the time delay of the double-pulse.

4.1 Effect of pulse shape

Pulse shaping has been used to control the free-electron excitation and thereby the breakdown threshold in surface ablation of dielectrics with ultra-short laser pulses[33]. In the internal modification of bulk dielectrics, however, pulse shaping has different effects because of plasma expansion towards the laser source.

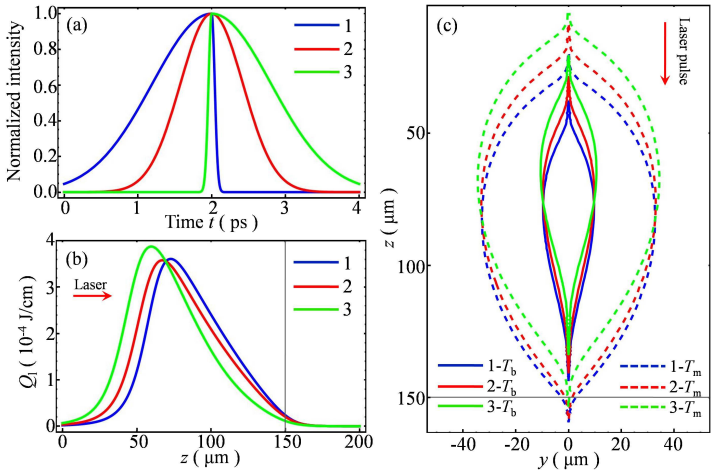

Figure 6. Effect of pulse shaping of picosecond lasers on internal modifications in bulk glass. (a) Three pulse shapes, (b) line density Q_l of the deposited energy along the z axis, and (c) isothermal lines of T_m and T_b on the cross-section of temperature distributions. "1", "2" and "3" indicate saw tooth shape, Gaussian shape and inverted saw tooth shape, respectively. 2.5 μJ, 1ps, 1064 nm, 500 kHz laser pulses with different pulse shapes are used. The red arrows in (b) and (c) indicate the laser incident direction. The focus of the laser beam is located at z =150 μm indicated by a thin gray line in (b) and (c).

Figure 6(a) shows the three chosen laser pulse shapes, i.e. saw-tooth shape, Gaussian shape and inversed saw-tooth shape, to induce internal modifications in the glass sample. The pulses with different shapes have the same peak intensity, pulse duration of 1 ps and pulse energy of 2.5 μJ. The other laser and material parameters are same as those given in Section 2.3. The corresponding line densities of the deposited energy for three pulse shapes are compared in Fig. 6(b) and the heat modification regions indicated by the two isothermal lines of T_m and T_b are in Fig. 6(c). The deposited energy distribution of the laser pulse with the saw-tooth shape is moved towards the focus while that with the inversed saw-tooth shape is shifted away from the focus with respect to that with the Gaussian shape. The internal modification size for the inversed saw-tooth shape is larger than those for the other two shapes. Therefore pulse shaping can be used to control the positions of energy deposition and internal modification in bulk glass by ultra-short laser pulses.

4.2 Free-electron density relaxation and accumulation

During the interaction of bulk glass with an ultra-short laser pulse, high-density free-electrons are generated. After the laser pulse, the free-electron density decreases because of electron-hole recombination. The decaying free-electron density will serve as the initial condition for the interaction of glass with the next pulse. When the time interval t_s between successive pulses is larger than the plasma relaxation time t_r, the free-electron density gets similar to that in the unexcited dielectrics and the interaction of dielectrics with the subsequent pulse is same to that with the former pulse. Otherwise, at the arrival of the subsequent pulse, the high-density initial free-electrons gain energy by inverse bremsstrahlung absorption and thereby induce cascade ionization without MPI; the threshold laser intensity for inducing nonlinear ionization and energy deposition is reduced. Thus extremely high repetition rate can induce the accumulation of free-electron density. Double-pulse train is a convenient solution to control the electronic accumulation and has been experimentally studied in the applications of microwelding[11, 12] and waveguide writing[34, 35]. The model presented in this work provides us a tool to numerically study the electronic excitation, relaxation and accumulation in the internal modification of bulk glass irradiated by double-pulse trains.

In the simulation, the bulk glass is irradiated by double-pulse trains at a repetition rate of 500 kHz. The double-pulse consists of two identical pulses with a time delay Δt. For each pulse, pulse duration is 10 ps and pulse energy is 1.23 μJ. The other laser and material parameters are same with those given in Section 2.3.

First we study the case of Δt = 100 ps and the peaks of the double-pulse are located at t = 20 ps and 120 ps, respectively. Laser-induced free-electron density distributions along the z axis at different time instants are shown in Fig. 7(a). The free-electron generation process induced by the first pulse is indicated by the dashed lines in Fig. 7(a) and is similar to that in Fig. 2(a). After 100ps, the second pulse interacted with the focal volume in bulk glass, specifically with the residual free-electrons. Thus the formation process of free-electron density induced by the second pulse is quite different from that by the first pulse. As indicated by the solid lines in Fig. 7(a), the first half of the second laser pulse is absorbed in the deposition region of the first pulse but the second half induces high-density free-electrons at the locations further towards the laser source by 20 μm. As the laser energy is deposited in a wider region along the z axis, the maximum free-electron density during the second pulse is smaller than that during the first pulse but the electronic damage region is extended.

In order to deeply understand the plasma formation induced by the double-pulse train, we study the temporal dynamics of free-electron density at four positions (z = 80 μm, 90 μm, 100 μm and 140 μm) on the z axis as shown in Fig. 7(b), which show the phenomena of electronic accumulation. When the second pulse arrives at the focal volume, the free-electron density induced by the first pulse has been decaying for around 100 ps. At t = 110 ps, i.e 10 ps ahead of the peak of the second pulse, the free-electron density is around 5×10^{18} cm^{-3} at z = 100 μm - 150 μm, 4×10^{17} cm^{-3} at z = 90 μm and 4×10^{16} cm^{-3} at z = 80 μm. As the cascade ionization rate is proportional to the product of laser intensity and free-electron density, due to the higher initial free-electron density and higher focused intensity, the free-electron density grows firstly at z = 140 μm at the leading edge of the pulse. When the laser intensity gets larger, high-rate cascade ionization increases the free electron density at z = 80 μm - 100 μm and the laser intensity is absorbed before reaching the focus. As the result, the maximum free-electron density at z = 90 μm and 100 μm exceeds the damage threshold density ρ_d, whereas the free-electron density at z = 140 μm does not reach ρ_d. The initial free-electron density at z = 80 μm is too small to get the free-electron density beyond ρ_d. Therefore when the initial free-electron density is larger than 4×10^{17} cm^{-3}, the electronic accumulation plays a crucial role in the plasma generation and expansion induced by the second pulse.

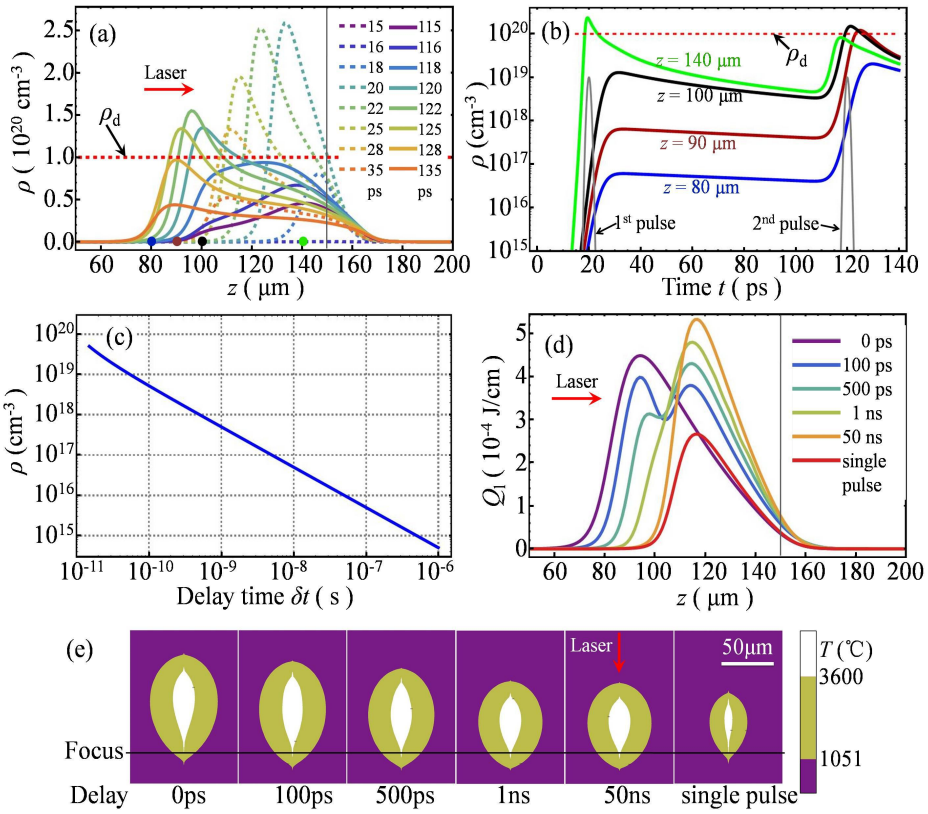

Figure 7. Effect of double-pulse trains on energy deposition and internal modification in bulk glass irradiated by picosecond lasers. (a) Distributions of free-electron density ρ along the z axis at different time instants and (b) temporal dynamics of free-electron density ρ at four positions on the z axis. (c) Relaxation of laser-induced free-electron density ρ with a value of 5×10^{19} cm^{-3} at Δt = 15 ps. (d) Line density distribution Q_l of the deposited energy along the z axis and (e) cross-sections of the modification regions at different time delays of the double-pulse. In (a) and (b), the time delay Δt of the double-pulse is 100ps. In (d) and (e), the time delay is given in the graphs and "0ps" and "single pulse" indicate the cases of a single-pulse train with a pulse energy of 2.46 μJ and 1.23 μJ, respectively. The red arrow in (a), (d) and (e) indicates the laser incident direction. The focus of laser beam is located at z = 150 μm indicated by a thin line in (a), (d) and (e). More details are described in the text.

After the first laser pulse, the laser intensity decreases to minimal and MPI and cascade ionization both vanish, so only recombination works. Therefore based on Eq. (1), the evolution of the free-electron density between the two pulses can be described as

$$\frac{\partial \rho(z,\Delta t)}{\partial \Delta t} = -\eta_{rec}\rho(z,\Delta t)^2, \tag{10}$$

where Δt > 15 ps. As shown in Fig. 7(a), at t = 35 ps, i.e. Δt = 15 ps, the free-electron density at z = 110 μm - 150 μm is around 5×10^{19} cm^{-3} while the laser intensity is negligible. The relaxation of laser-induced free-electron density with an initial value of 5×10^{19} cm^{-3} is numerically studied with Eq. (10) as shown in Fig. 7(c). The free-electron density decays to around 10^{17} cm^{-3} in a time scale of 1 ns. Therefore the times delay Δt of the double-pulse is taken from 0 ps to 50 ns to study the electronic accumulation effect on the interaction of bulk glass with the second pulse. The line density distributions of the deposited energy induced by the double-pulse train with different time delays are shown in Fig. 7(d). With increasing Δt, the deposited energy distribution of the second pulse is moving towards the focus because the initial free-electron density of bulk glass at the arrival of the second pulse is decaying.

Using the deposited energies in Fig. 7(d) as line heat sources, we get the cross-sections of the modification regions in bulk glass irradiated by the double-pulse train with different time delays as shown in Fig. 7(e). With increasing Δt, the size of the modification region along the z axis is decreasing and the shape of outer contour gets close to a regular circle, whereas the inner structure is always a tear-drop shape with a slight modulation. When Δt > 1 ns, the deposited energy

and modification region are converged and the impact of the free-electron density induced by the first pulse on the energy deposition of the second pulse can be negligible. In addition, the case of the single pulse train is also given for comparison.

The absorptivity for the first pulse in the double-pulse train is a constant of 65.1%. For the second pulse, however, the absorptivity A depends on the delay Δt of the double-pulse and is evaluated to be A = 90.5%, 88.5%, 81.1%, 73.4% and 65.1% corresponding to the delay Δt of 0 ps, 100 ps, 500 ps, 1 ns and 50 ns. Therefore, by varying the time delay of the double-pulse, one can control the energy deposition of the second pulse and thereby the size of the internal modification region.

From Figs. 7(d) and 7(e), we can get that the size of the heat-affect zone at Δt = 0 ps is larger than that at Δt > 0 ps as well as the optical absorptivity. The reason is that, as concluded from Fig. 2, cascade ionization is dominant in the plasma formation with a 10-ps laser pulse. If pulse duration is shorter, e.g.100 fs, the electron plasma is mainly generated via MPI or tunneling ionization instead of cascade ionization, thus the peak of the plasma density comes later than the pulse peak[18]. Therefore the effect of the time delay of double pulse on the internal modification will be different from that with 10-ps pulses. For example, in laser welding of Foturan glass with 360-fs double-pulse train, Sugioka et al. [11, 12] reported that the size of the heat affected zone increased as the delay time was increased from 0 ps to 15 ps and then decreased for larger decay times.

4.3 Heat accumulation and thermal ionization

In the internal interaction volume of bulk glass with high repetition rate ultra-shot laser pulses, heat accumulation results in high temperatures up to several thousand degrees [14-16] as shown in Fig. 4(a). Then thermal ionization becomes crucial to produce high-density free-electrons[9], which is another source of the initial free-electron density for the plasma formation induced by subsequent pulses. Therefore heat accumulation and thereby thermal ionization can also lead to electronic accumulation.

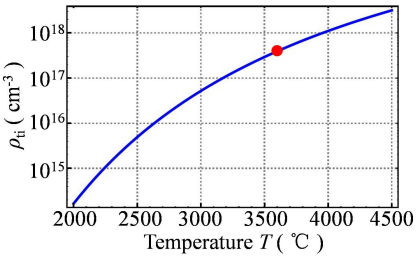

Figure 8. Free-electron density ρ_{ti} induced by thermal ionization in glass as a function of sample temperature. The bound electron density is calculated to be 2.5×10^{22} cm^{-3}. The red spot on the curve indicates the thermal-ionized free-electron density at the temperature of 3600°C.

Assuming the molecules of glass are in a thermalized Maxwell-Boltzmann distribution [9, 26], the free-electron density ρ_{ti} induced by thermal ionization as a function of sample temperature is shown in Fig. 8. When the temperature T reaches 3600 °C, the free-electron density is around 4×10^{17} cm^{-3}, which is the critical value to initialize the electronic accumulation (see Section 4.2). Therefore in the volume where T > 3600 °C, the high-density thermal-ionized free-electrons serve as the seed electrons for cascade ionization and the free-electron density rapidly rises beyond the threshold value ρ_d for the electronic damage. The temperature of 3600 °C is a trigger for electronic accumulation and damage. The electronic damage region increases when the isothermal line of 3600 °C expands in the y-z plane because of heat diffusion. Therefore the electronic damage causes the inner structure in the modification region and heat accumulation and diffusion induces the expansion of the inner structure. Because the electronic damage occurs in a shorter time scale than thermal modification, the electronic damage region (the darker inner structure) could be further modulated because of phase transition and glass element flow [31] and thereby covered by the heat affected zone (the outer molten region) as we have found in surface ablation of borosilicate glass [25]. Based on the above numerical analysis, the inner structure in the modification region is the electronic damaged zone, which is consistent with the heat affected zone where T > 3600 °C.

As a summary of the above discussions, we give a review of the main physical processes of the internal modification in bulk glass with high repetition rate picosecond laser pulses and discuss two types of electronic accumulation mechanisms. After the interaction of glass with laser pulse, the free-electron density gets to be negligible in the relaxation time t_r, which is in a scale of 1 ns. The absorbed energy via free-electrons heats the interaction volume and raises the

temperature and thermal diffusion time t_d is in a scale of microseconds [15]. When the time interval t_s of successive pulses is less than t_r, electronic accumulation occurs and the absorptivity for subsequent pulses is increased. This is referred as the first type of electronic accumulation. When $t_r < t_s < t_d$, only the heat accumulation occurs and the temperature increases with pulse number. When the temperature in the interaction volume exceeds 3600 °C, thermal ionization provides the initial free-electron density larger than 4×10^{17} cm^{-3} for the interaction of glass with the subsequent pulses. This is referred as the second type of electronic accumulation. Therefore heat accumulation and electronic accumulation induced by thermal ionization are combined in the internal modification of bulk glass with high repetition rate ultra-short laser pulses. Electronic accumulation reduces the threshold intensity for nonlinear ionization, extends the absorption region in the axial and transverse directions and increases the deposited energy.

5. CONCLUSIONS

In summary, we have numerically investigated the internal modification in bulk glass irradiated by picosecond laser pulses at a repetition rate of 500 kHz. We have developed a numerical model describing free-electron dynamics, nonlinear energy deposition and thermal diffusion. Cascade ionization dominates in laser-induced plasma formation; the maximum free-electron density produced in the interaction volume was shown to saturate around 3×10^{20} cm^{-3}, which is well below the breakdown threshold density (10^{21} cm^{-3} for 1064 nm). The simulated cross-sections of heat modification regions, as well as the nonlinear absorptivity, agreed quite well with the experimental results at various pulse energies. The length of the inner structure was accurately estimated by the damage threshold free-electron density; thus the forming mechanism of the inner structure in the modification region was contributed to the electronic damage considering the combined effect of heat accumulation, thermal ionization and electronic accumulation.

By pulse shaping, the energy deposition and the internal modification in bulk glass were modulated. Relaxation and accumulation of free-electron density have been discussed based on a double-pulse train. By varying the time delay of the double-pulse from 0 ps to 50 ns, the absorptivity for the second pulse was tuned from 90.5% and 65.1%; the energy deposition of the second laser pulse and the internal modification can be controlled continuously. The threshold free-electron density for electronic accumulation is 4×10^{17} cm^{-3}, which is corresponding to the free-electron density induced by thermal ionization at the temperature of 3600 °C. The relation of heat accumulation, thermal ionization and electronic accumulation was discussed to explain the formation mechanism of the inner structure in the modification region. Based on the comparisons of the time interval of successive pulses with the relaxation time of laser-induced free-electron density and the thermal diffusion time, we revealed two electronic accumulation mechanisms in the internal modification of bulk with high repetition rate ultra-short laser pulses.

REFERENCES

[1] Gattass, R. R. and Mazur, E., "Femtosecond laser micromachining in transparent materials," Nat. Photonics 2, 219-225 (2008).

[2] Schaffer, C. B., Brodeur, A., Garcia, J. F. and Mazur, E., "Micromachining bulk glass by use of femtosecond laser pulses with nanojoule energy," Opt. Lett. 26, 93-95 (2001).

[3] Eaton, S. M., Zhang, H., Herman, P. R., Yoshino, F., Shah, L., Bovatsek, J. and Arai, A. Y., "Heat accumulation effects in femtosecond laser-written waveguides with variable repetition rate," Opt. Express 13, 4708-4716 (2005).

[4] Osellame, R., Chiodo, N., Maselli, V., Yin, A., Zavelani-Rossi, M., Cerullo, G., Laporta, P., Aiello, L., De Nicola, S., Ferraro, P., Finizio, A. and Pierattini, G., "Optical properties of waveguides written by a 26MHz stretched cavity Ti:sapphire femtosecond oscillator," Opt. Express 13, 612-620 (2005).

[5] Gattass, R. R., Cerami, L. R. and Mazur, E., "Micromachining of bulk glass with bursts of femtosecond laser pulses at variable repetition rates," Opt. Express 14, 5279-5284 (2006).

[6] Eaton, S. M., Zhang, H., Ng, M. L., Li, J., Chen, W., Ho, S. and Herman, P. R., "Transition from thermal diffusion to heat accumulation in high repetition rate femtosecond laser writing of buried optical waveguides," Opt. Express 16, 9443-9458 (2008).

[7] Miese, C., Withford, M. J. and Fuerbach, A., "Femtosecond laser direct-writing of waveguide Bragg gratings in a quasi cumulative heating regime," Opt. Express 19, 19542-19550 (2011).

[8] Tamaki, T., Watanabe, W. and Itoh, K., "Laser micro-welding of transparent materials by a localized heat accumulation effect using a femtosecond fiber laser at 1558 nm," Opt. Express 14, 10460-1048 (2006).

[9] Miyamoto, I., Cvecek, K. and Schmidt, M., "Evaluation of nonlinear absorptivity in internal modification of bulk glass by ultrashort laser pulses," Opt. Express 19, 10714-10727 (2011).
[10] Miyamoto, I., Cvecek, K., Okamoto, Y., Schmidt, M. and Helvajian, H., "Characteristics of laser absorption and welding in FOTURAN glass by ultrashort laser pulses," Opt. Express 19, 22961-22973 (2011).
[11] Sugioka, K., Iida, M., Takai, H. and Micorikawa, K., "Efficient microwelding of glass substrates by ultrafast laser irradiation using a double-pulse train," Opt. Lett. 36, 2734-2736 (2011).
[12] Wu, S., Wu, D., Xu, J., Hanada, Y., Suganuma, R., Wang, H., Makimura, T., Sugioka, K. and Midorikawa, K., "Characterization and mechanism of glass microwelding by double-pulse ultrafast laser irradiation," Opt. Express 20, 28893-28905 (2012).
[13] Zimmermann, F., Richter, S., Doering, S., Tuennermann, A. and Nolte, S., "Ultrastable bonding of glass with femtosecond laser bursts," Appl. Opt. 52, 1149-1154 (2013).
[14] Sakakura, M., Shimizu, M., Shimotsuma, Y., Miura, K. and Hirao, K., "Temperature distribution and modification mechanism inside glass with heat accumulation during 250 kHz irradiation of femtosecond laser pulses," Appl. Phys. Lett. 93, 231112 (2008).
[15] Yoshino, T., Matsumoto, M., Ozeki, Y. and Itoh, K., "Energy-dependent temperature dynamics in femtosecond laser microprocessing clarified by Raman temperature measurement," Proc. SPIE 8249, 82491D (2012).
[16] Hermans, M., Gottmann, J. and Schiffer, A., "In-situ diagnostics on fs-laser induced modification of glasses for selective etching," Proc. SPIE 8244, 82440E (2012).
[17] Shimizu, M., Sakakura, M., Ohnishi, M., Shimotsuma, Y., Nakaya, T., Miura, K. and Hirao, K., "Mechanism of heat-modification inside a glass after irradiation with high-repetition rate femtosecond laser pulses," J. Appl. Phys. 108, 073533 (2010).
[18] Vogel, A., Novak, J., Hüttman, G. and Paltauf, G., "Mechanisms of femtosecond laser nanosurgery of cells and tissues," Appl. Phys. B 81, 1015-1047 (2005).
[19] Sudrie, L., Couairon, A., Franco, M., Lamouroux, B., Prade, B., Tzorzakis, S. and Mysyrowicz, A., "Femtosecond laser-induced damage and filamentary propagation in fused silica," Phys. Rev. Lett. 89, 186601 (2002).
[20] Arnold, C. L., Heisterkamp, A., Ertmer, W. and Lubatschowski, H., "Computational model for nonlinear plasma formation in high NA micromachining of transparent materials and biological cells," Opt. Express 15, 10303-10317 (2007).
[21] Popov, K. I., McElcheran, C., Briggs, K., Mack, S. and Ramunno, L., "Morphology of femtosecond laser modification of bulk dielectrics," Opt. Express 19, 271-282 (2011).
[22] Jiao, J. and Guo, Z., "Modeling of ultrashort pulsed laser ablation in water and biological tissues in cylindrical coordinates," Appl. Phys. B 103, 195-205 (2011).
[23] Rayner, D. M., Naumov, A. and Corkum, P. B., "Ultrashort pulse non-linear optical absorption in transparent media," Opt. Express 13, 3208-3217 (2005).
[24] Burakov, I. M., Bulgakova, N. M., Stoian, R., Mermillod-Blondin, A., Audouard, E., Rosenfeld, A., Husakou, A. and Hertel, I. V., "Spatial distribution of refractive index variations induced in bulk fused silica by single ultrashort and short laser pulses," J. Appl. Phys. 101, 043506 (2007).
[25] Sun, M., Eppelt, U., Russ, S., Hartmann, C., Siebert, C., Zhu, J. and Schulz, W., "Numerical analysis of laser ablation and damage in glass with multiple picosecond laser pulses," Opt. Express 21, 7858-7867 (2013).
[26] Kennedy, P. K., "A first-order model for computation of laser-induced breakdown thresholds in ocular and aqueous media: Part I – Theory," IEEE J. Quant. Electron. 31, 2241-2249 (1995).
[27] Yoshino, F., Shah, L., Fermann, M., Arai, A. and Uehara, Y., "Micromachining with a high repetition rate femtosecond laser," J. Laser Micro/Nanoeng. 3, 157-162 (2008).
[28] Schott D263 Material Information Sheet http://www.schott.com/advanced_optics/english/download/.
[29] Sun, Q., Jiang, H., Liu, Y., Zhou, Y., Yang, H. and Gong, Q., "Relaxation of dense electron plasma induced by femtosecond laser in dielectric materials," Chin. Phys. Lett. 23, 189-192 (2006).
[30] Gulley, J. R., Winkler, S. W., Dennis, W. M., Liebig, C. M. and Stoian, R., "Interaction of ultrashort-laser pulses with induced undercritical plasmas in fused silica," Phys. Rev. A 85, 013808 (2012).
[31] Shimizu, M., Sakakura, M., Ohnishi, M., Yamaji, M., Shimotsuma, Y., Hirao, K. and Miura, K., "Three-dimensional temperature distribution and modification mechanism in glass during ultrafast laser irradiation at high repetition rates," Opt. Express 20, 934-940 (2012).

[32] Hoehm, S., Rosenfeld, A., Krueger, J. and Bonse, J., "Femtosecond laser-induced periodic surface structures on silica," J. Appl. Phys. 112, 014901 (2012).
[33] Englert, L., Rethfeld, B., Hagg, L., Wollenhaupt, M., Sarpe-Tudoran, C. and Baumert, T., "Control of ionization processes in high band gap materials via tailored femtosecond pulses," Opt. Express 15, 17855-17862 (2007).
[34] Nagata, T., Kamata, M. and Obara, M., "Optical waveguide fabrication with double pulse femtosecond lasers," Appl. Phys. Lett. 86, 251103 (2005).
[35] Wortmann, D., Ramme, M. and Gottmann, J., "Refractive index modification using fs-laser double pulses," Opt. Express 15, 10149-10153 (2007).